

Article

Nanoindentation on the Transformation of LPSO Phases during Different Solution Heat Treatments in an Mg-Dy-Nd-Zn-Zr Alloy

Petra Maier ^{1,2,*} , Merle Schmahl ³, Benjamin Clausius ¹, Charis Joy ¹ and Claudia Fleck ³ ¹ School of Mechanical Engineering, University of Applied Sciences Stralsund, 18435 Stralsund, Germany² Department of Mechanical Engineering Sciences, Lund University, 22100 Lund, Sweden³ Institute of Materials Science and Technology, Technische Universität Berlin, 10623 Berlin, Germany

* Correspondence: petra.maier@hochschule-stralsund.de; Tel.: +49-3831-456914

Abstract: The objective of this study is the investigation of nanomechanical properties using nanoindentation of extruded and heat-treated Mg-Dy-Nd-Zn-Zr, with an emphasis on the transformation of long-period stacking-ordered (LPSO) phases. Solution heat treatment was performed with different heat treatment for durations on hot extruded Mg-Dy-Nd-Zn-Zr to monitor the transformation of LPSO phases, as well as to keep track of microstructural changes. The initial fine-grained microstructure, with blocky and lamellar LPSO structures within the matrix, first transformed into coarser grains with fewer LPSO lamellae, which then increased in amount again at higher annealing duration. The blocky LPSO phases, which have the highest hardness compared to the matrix grains with and without LPSO lamellae, consistently decrease in quantity, as so does the trend in their hardness value. The Mg matrix grains with LPSO lamellae show a lower hardness compared to the Mg matrix grains without or with a just few lamellar LPSO phases, and increase in quantity at long annealing durations. The overall hardness of the microstructure is essentially determined by the LPSO lamellae-containing grains and reaches a peak at 24 h. There is another peak found for the grain size values; however, this is at later annealing duration, at 72 h. The reduction in grain size towards longer annealing durations goes along with a reactivated formation of LPSO lamellae.

Keywords: nanoindentation; nanohardness; LPSO phase transformation; dissolution; precipitation

Citation: Maier, P.; Schmahl, M.; Clausius, B.; Joy, C.; Fleck, C. Nanoindentation on the Transformation of LPSO Phases during Different Solution Heat Treatments in an Mg-Dy-Nd-Zn-Zr Alloy. *Crystals* **2022**, *12*, 1673. <https://doi.org/10.3390/cryst12111673>

Academic Editor: Umberto Prisco

Received: 20 October 2022

Accepted: 14 November 2022

Published: 20 November 2022

Publisher's Note: MDPI stays neutral with regard to jurisdictional claims in published maps and institutional affiliations.



Copyright: © 2022 by the authors. Licensee MDPI, Basel, Switzerland. This article is an open access article distributed under the terms and conditions of the Creative Commons Attribution (CC BY) license (<https://creativecommons.org/licenses/by/4.0/>).

1. Introduction

Magnesium (Mg) alloys containing long-period stacking-ordered (LPSO) phases are receiving growing attention due to their improvement of mechanical and corrosion properties. This is change based on unique microstructural features which are easily adapted by post-heat treatment and manufacturing routes, like extrusion and equal channel angular pressing (ECAP) [1–8]. Various Mg-rare earth (RE)-containing alloys, like Mg-Y-Zn-based alloys [9–14], Mg-Gd-based alloys [15–23] and Mg-Dy-Ni-based alloys [24,25], have been studied in cast and extruded states. The appearance of LPSO phases depends on the ratio of RE to Zn as well as the alloy composition and processing in general. The LPSO phases arrange periodically in the Mg basal planes due to restricted Zn/RE distributions at the close-packed atomic layers, forming a well-ordered structure, for example a local ABCA (fcc) stacking [26]. They are found to be either block-shaped within the grain and/or at the grain boundaries, or needle-like (lamellar)-shaped inside the grains [27]. The transformation of the morphology of these LPSO phases (named 14H-LPSO phases in lamellar shape and 18R-LPSO in block-shape) by thermo-mechanical treatment or post-heat treatment, which depends on their initial appearance, is well studied. Blocky LPSO phases can transform into lamellar LPSO phases, and both phase formations can dissolve in and precipitate from the Mg matrix during aging treatment. The possible change of their periodical intervals and the role of stacking faults as diffusion paths are well described [4,5,10,18,22,24,25,28].

Ding et al. [17] conclude that, following solid solution heat treatment of as-cast Mg–Gd–Zn–Zr at 698–813 K, a novel lamellar phase with a 14H-type LPSO structure was formed from the dendritic β -phase already existing in the Mg matrix, in addition to the initial coherent fine lamellae of type 14H-LPSO. Liu et al. [10] summarize that during annealing at 773 K, 14H-LPSO lamellae first precipitates in cast Mg–Y–Zn and then dissolves into the Mg matrix, while blocky 18R-LPSO phases display no obvious change. The formation of 14H-LPSO lamellae in the cast alloy during annealing follows the reaction process whereby 18R-LPSO, plus Mg matrix, transforms into 14H-LPSO lamellae. As for the extruded alloy, the 14H precipitates from the supersaturated solid solution stage and grows continuously with increasing annealing time, while 18R gradually dissolves. The extruded alloy exhibits an Mg matrix/14H-LPSO phase dual microstructure when annealed.

Zhang et al. [4] describe the microstructure of Mg–Gd–Y–Zn–Zr, consisting of both grains containing LPSO lamellae and grains free of them. They state that no obvious contrast of lamellar LPSO phases in microscopy images can be found, which indicated that these phases might dissolve. A microstructure of Mg grains with and without LPSO lamellae has also been found for Mg–Gd–Y–Zn–Zr in the study by Wang et al. [23]. Most of the grains have dense lamellar LPSO phases inside, which are arranged in parallel to each other. In brighter Mg grains, no LPSO lamellae were visible—an observation which agrees with other studies on Mg–Gd–Y–Zn–Zr [11,19,20]. The transformation of blocky LPSO phases into lamellar ones has also been found in [5,9,15,16]—a process conducted either by forging, extrusion or post-heat treatment.

Yuan et al. [25] investigated the morphological evolution of LPSO phases in Mg–Dy–Ni caused by solid solution treatment, different cooling conditions and precipitation hardening. During solution heat treatment, dot-shaped, block, fine lamellar and rod-shaped LPSO phases precipitated in the as-cast Mg matrix. For continuous cooling conditions, the fine LPSO lamellae phase generally formed within the grains with increasing volume fraction and blocky LPSO phase coarsened with increasing cooling time. For discontinuous cooling conditions, the dot-shaped LPSO grew into the rod-shaped phase.

Xu et al. [18] also studied different cooling conditions on cast Mg–Gd–Y–Zn–Zr: furnace cooling and quenching after homogenization. While the majority of the eutectic phases were dissolved into the Mg matrix, a small amount of block-shaped LPSO phases remained at the grain boundaries, especially at the triple junctions. The plate-shaped 14H-LPSO phases precipitated and grew across the whole grains during slow cooling. After quenching supersaturated solid solution, Mg grains without visible precipitation were seen. After slow cooling, no obvious grain growth was found, which potentially would have stemmed from the effective pinning of the grain boundaries by both block-shaped LPSO phases and the plate-shaped 14H-LPSO phases inside the grains.

The microstructure and mechanical properties of an extruded Mg–Dy–Ni alloy have been studied by Bi et al. [2]. The as-extruded alloy was mainly composed of Mg matrix grains, the Mg_2Dy phase, 18R-LPSO phases distributed along the extrusion direction and small amounts of fine 14H-LPSO phase in the grain interior. During aging, two hardness peaks were observed: the first one mainly originated from the high number of blocky 18R-LPSO phases in conjunction with the precipitation of underaged 14H-LPSO phase, and the second one mainly arose from the precipitation of a high-volume fraction of 14H-LPSO phases in the grain interior.

Kittner et al. [12] found that annealing of twin-roll cast Mg–Zn–Zr alloy led to partial dissolution of the initial continuous network of the LPSO phases into the Mg matrix when quenched in water and that the morphology changed significantly: to block-shaped at 500 °C for 2 h and to a globular and rod-like shape at 525 °C for 6 h. The volume fraction of the LPSO phase decreased with increasing temperature. After heat treatment at 525 °C, fine 14H-LPSO lamellae precipitated within the Mg matrix grains at the expense of the dissolution of the network-shaped 18R-LPSO phase. Cooling at a low cooling rate in the air then led to the formation of the fine lamellae of an LPSO structure—which could be assigned to the 14H-LPSO phase—and here its precipitation was not suppressed.

Wang et al. [14] studied the transformation of LPSO phases in an Mg-Y-Er-Zn-Zr alloy during heat treatment. Prior to heat treatment, the alloy consisted of an Mg matrix and 14H-LPSO lamellae. After heat treatment at 510 °C, the lamellae shortened, and their content decreased. Upon 8 h heat treatment, blocky 18R-LPSO phases formed at the grain boundaries while the 14H-LPSO lamellae disappeared.

Schuh [29] stated already in 2006 that nanoindentation has become a commonplace tool for the measurement of mechanical properties at small scales and since then Mg alloys have also been nanomechanically analyzed [30–32]. Studying the effects of Mn on the microhardness, HV0.01, of LPSO phases containing Mg-Zn-Y shows a significant higher hardness for the 18R-LPSO phases compared to the Mg matrix—in the solid solution state slightly less hard compared to the as-cast state [33]. Research on ZrB₂-modified Mg-Zn-Y-Mn shows with a nanohardness value of approximately 1.6 GPa a higher nanohardness at an applied load of 5 mN of the blocky LPSO phases compared to the Mg matrix with 1.0 GPa [34]. Individual microhardness measurements on Mg-Gd-Y-Zn-Zr [35] also show a higher hardness of the blocky 18R-LPSO phases (105 HV) compared to the Mg matrix-containing 14H-LPSO lamellae (71 HV). In terms of microhardness, the LPSO phases forming in as-cast Mg-2.5Y-1Ce-0.5Mn have been found to be twice as hard the Mg matrix [36].

The Mg-Dy-Nd-Zn-Zr alloy used in this study is high in the Dy content (>10 wt.%) and was developed specifically for absorbable implants by MeKo Manufacturing e.K. in Sarstedt and the Helmholtz-Zentrum Hereon in Germany [37]. The alloy shows good strength and ductility, high elasticity and excellent fatigue life in air [38,39]. In combination with other alloying elements, such as Gd, Zr, and Nd, Dy, having a high solubility in Mg, both the mechanical and corrosion properties can be adjusted by heat treatment [40,41].

Ahlers et al. [42] previously investigated the influence of the cooling conditions on the morphology of the LPSO phases in cast Mg-Dy-Nd-Zn-Zr. Grains became larger with increasing heat treatment duration and slow cooling led to additional grain growth. Slow cooling supported the development of LPSO lamellae, which transformed from the blocky LPSO phases during the cooling process. Crack growth in the alloy used in this study was investigated in [43] with attention to the role of LPSO phases. Solution heat treatment changed the initial fine-grained microstructure, consisting of grain boundary blocky LPSO and lamellar LPSO structures within the matrix, into coarser grains of less lamellar and blocky LPSO phases. Crack initiation and propagation was found to be influenced by twin boundaries and LPSO lamellae being surrounded by softer Mg matrix. The blocky LPSO phases hindered crack growth due to their higher hardness; however, their amount decreased with increasing heat treatment duration. The Mg matrix in between LPSO lamellae was found to be less hard than the Mg matrix in grains free of LPSO lamellae, where solid solution strengthening was expected.

It becomes clear that the general transformation possibilities between the phases have been widely researched, and understood in turn to some degree. However, new alloying possibilities and fabrication routes still leave some questions unanswered. How the phases change the mechanical properties on the macro-scale is also essentially known. In contrast, much less is known about the influence of heat treatments on the local mechanical properties. Therefore, this study aims to quantitatively investigate the change in microstructure and examine the nanohardness of each phase influenced by solid solution, testing how sensitively nanohardness can measure even minor hardness changes due to different cooling rates.

2. Materials and Methods

The Mg-Dy-Nd-Zn-Zr alloy in this study, extruded in tubes, consists of 12.63 wt.% Dy, 1.05 wt.% Nd, 0.94 wt.% Zn and 0.075 wt.% Zr, and was analyzed by X-ray micro fluorescence and spark optical emission spectroscopy [43]. The manufacturing route of the tubes can be found in detail in [43]. The hot-extruded Mg-Dy-Nd-Zn-Zr alloy was solution heat treated for 0.5 h, 1 h, 24 h, 72 h, 96 h or 120 h at 500 °C, followed by water quenching in 55 °C warm water. For the solution heat treatment duration of 0.5 h and 1 h also, cooling

in air was applied. The samples for nanoindentation were cut from the extruded tubes and the cross-section was used for hardness measurements and microstructure characterization.

The samples were prepared by grinding with SiC paper to a grit size of 4000, followed by polishing with 3 and 1 μm water-free diamond paste and 0.25 μm OPS colloidal silica. The samples were then cleaned with ethanol and dried with hot air. The microstructure was developed by etching in a solution of 4.2 g picric acid, 10 mL acetic acid, 10 mL distilled water, and 70 mL ethanol for a few seconds only. Micrographs were obtained with a Leica DMI8 (Leica Microsystems GmbH, Wetzlar, Germany). IMAGIC IMS software was used to take grain size measurements, applying the line intercept technique.

Quasi-static nanoindentation tests were carried out using a TI 950 TriboIndenter (Bruker, MA, USA) equipped with a Berkovich tip. The tests were conducted in a load-controlled mode and a trapezoidal load function: the maximum force was 1 mN, and loading/holding/unloading lasted 5 sec each. Grids of 15×15 indents were taken with a grid spacing of 8 μm . Force–displacement curves were monitored. The indents were visualized using the TI 950 TriboIndenter in either the scanning probe microscopy imaging mode, the Leica DMI8 light microscope or a scanning electron microscope (SEM; VEGA4 GMU, TESCAN, Brno, Czech Republic). Each indent could thus be assigned to the location of the hardness measurement. The overall hardness values, the average of all hardness values, shows the hardness of all the grains measured without the blocky LPSO phases.

3. Results

Figure 1 shows representative micrographs of the Mg-Dy-Nd-Zn-Zr alloy in an as-extruded state (Figure 1a), and after heat treatment at 500 °C for 0.5 h, 1 h, 24 h, 72 h, 96 h and 120 h followed by quenching in 55 °C warm water (Figure 1b–g). The majority of the grains in the as-extruded state contain LPSO lamellae within the grains (grey and darker grey grains). Some grains appear very bright and are expected to be free of lamellae—the as-extruded microstructure also shows precipitates and grain boundary LPSO phases. A coarser-grained microstructure was found after solution heat treatment. The grains reveal microstructural features, such as the lamellar LPSO structures with the Mg matrix and blocky LPSO phases within the grains and at the grain boundaries. Some grains show twin boundaries (for example in Figure 1b). The number of grains containing lamellar LPSO increases in quantity after solution heat treatment for 96 h and 120 h. The number of blocky LPSO phases decrease further towards 120 h—the study in [43] has already presented a decrease between 24 h and 72 h and the images in Figure 1b and c clearly show the highest amount of blocky LPSO among the heat-treated states.

The micrographs in Figure 2 support the statements on the appearance of lamellae-free and lamellae-containing grains, as well as those about the grains in the heat-treated states. The brighter microstructural feature-free grains in the light microscopy images (Figure 2c,d,f) do not show LPSO lamellae. If they do show them, it is only very few, and the same is true of the grains in the SEM images (Figure 2a,b,e). The images in Figure 2b and c show the same details in the microstructure of the heat-treated samples at 500 °C for 0.5 h, and so does Figure 2e,f for the heat-treated samples at 500 °C for 96 h.

The micrographs in Figure 2 are taken at the grit area, seen by 15×15 small indents in horizontal and vertical lines—in Figure 2d the indents are marked in red. Indents at interfaces and grain boundaries are eliminated in calculating average nanohardness values. This is also the case indents near or on the RE-hydrides, seen as white cubical particles in the SEM images, as see Figure 2a and as is correlated to [44]. Since these particles are hard but cannot be indented without false values (sliding off), their values are not taken into account.

The SEM images in Figure 3a and b show once more the different appearance of Mg matrix grains containing LPSO lamellae (here named “Matrix lamellae”) and lamellae free grains (here named “Matrix solid”). The force–displacement curves in Figure 3c are representative curves of blocky LPSO phases, the Mg matrix in between the LPSO lamellae and the Mg matrix free of LPSO lamellae (solid). The highest displacement is seen for the

Mg matrix in the LPSO lamellae-containing grains, and the lowest displacement is found for the blocky LPSO phases. All curves show small pop-ins. Attempting to assign the amount of pop-ins to the microstructural feature has not revealed a trend of either more or less regarding indenting obvious LPSO lamellae. Lamellae will be responsible for the pop-ins, but so will strain bursts due to dislocation movement in other microstructural regions. Blocky LPSO phases also show no outstanding characteristic features. Figure 3b also presents twin boundaries. The microstructure around twins shows a high scattering of hardness values, and obvious statistical outliers are not considered.

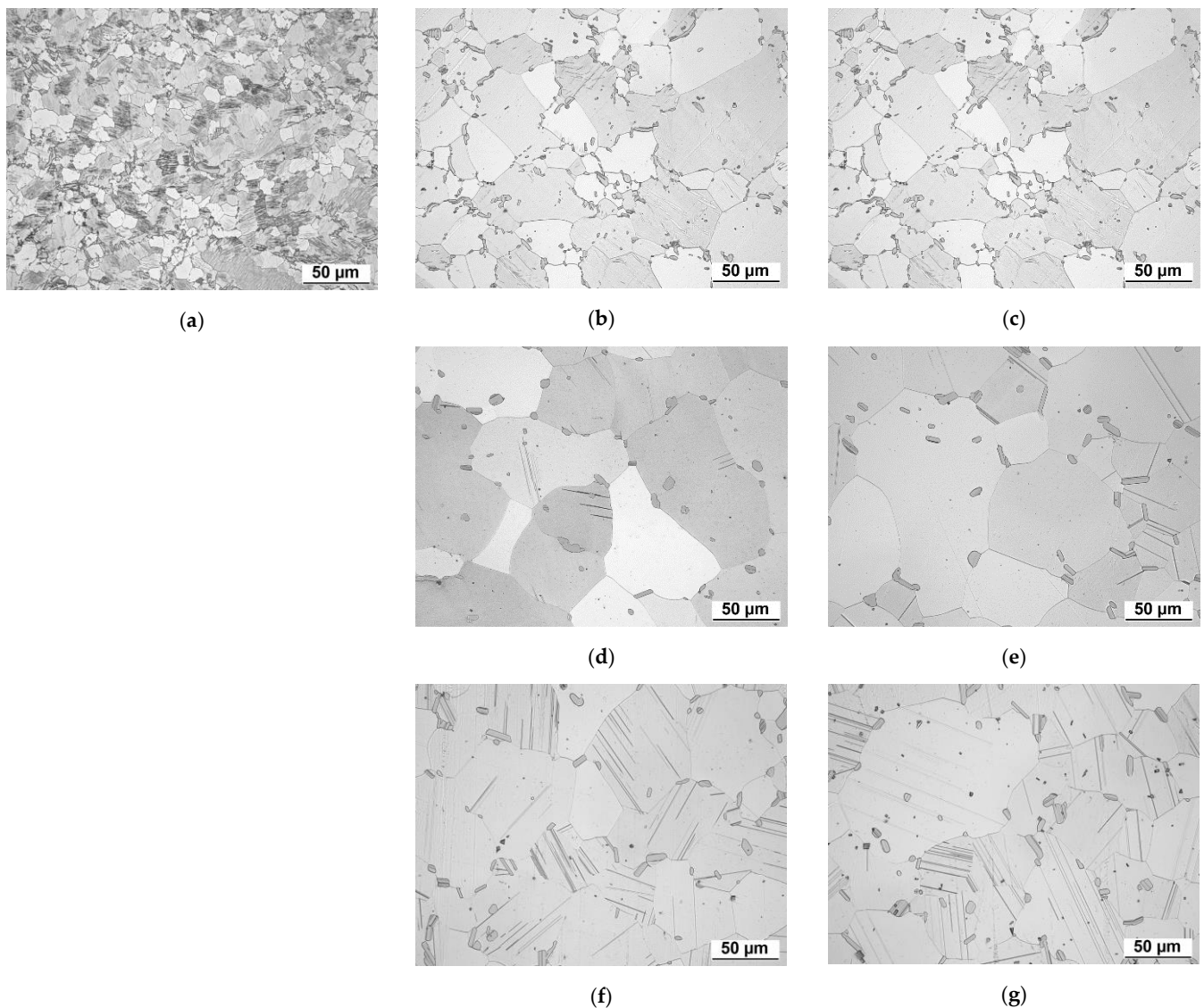


Figure 1. Light micrographs of Mg-Dy-Nd-Zn-Zr alloy in (a) as-extruded state, showing LPSO lamellae within the grains, precipitates and grain boundary LPSO phases after heat treatment at 500 °C for (b) 0.5 h, (c) 1 h, (d) 24 h, (e) 72 h, (f) 96 h and (g) 120 h, followed by quenching in 55 °C warm water, showing LPSO lamellae within Mg matrix grains and blocky LPSO within grains and at grain boundaries of different quantities.

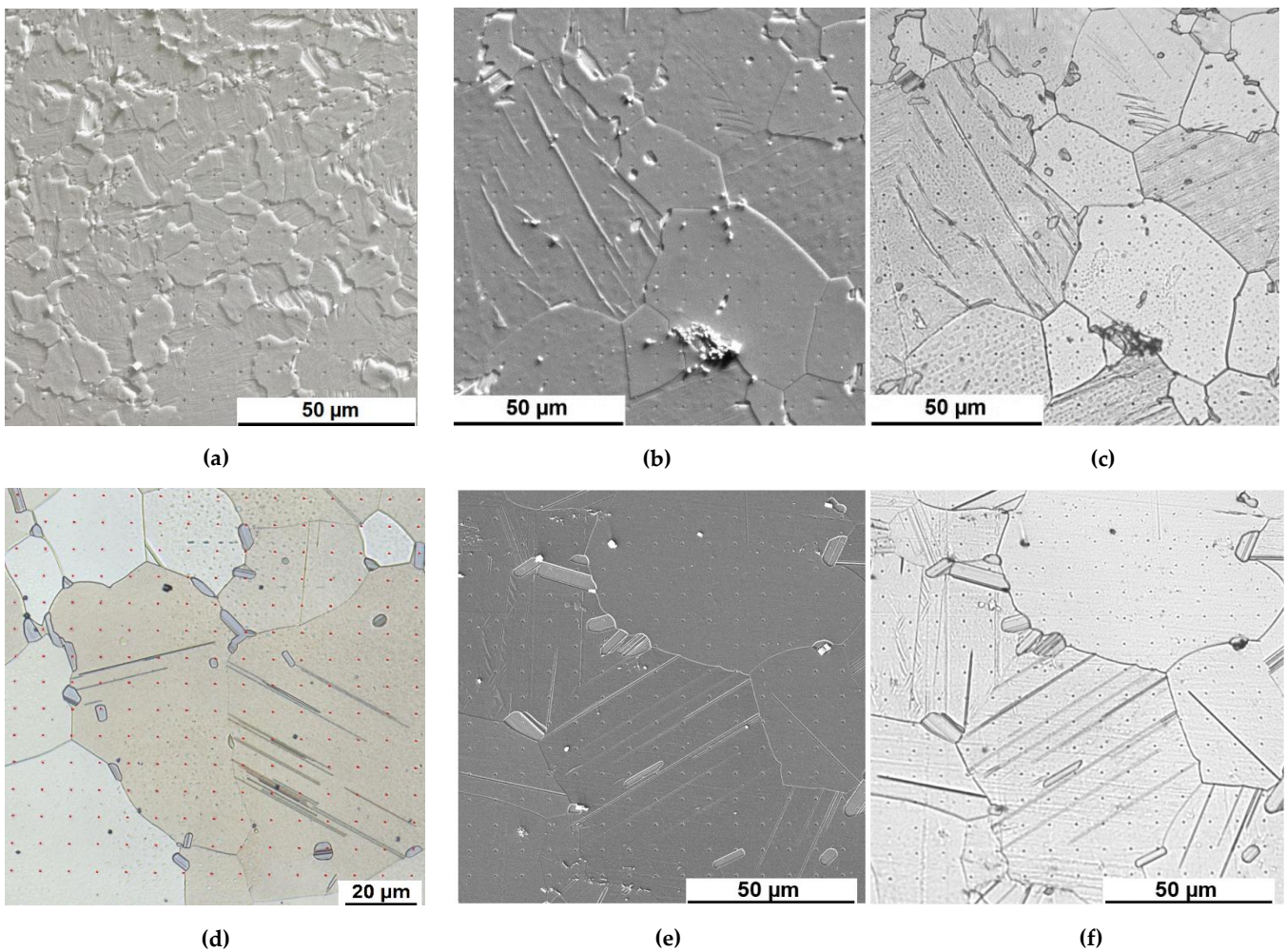


Figure 2. Micrographs of Mg-Dy-Nd-Zn-Zr alloy in extruded state (a), after heat treatment at 500 °C for 0.5 h (b,c), 24 h (d) and 96 h (e,f) followed by quenching in 55 °C warm water, (a,b,e) SEM and (c,d,f) light microscopy, all images show the grits of 15 × 15 indents, in (d) marked in red.

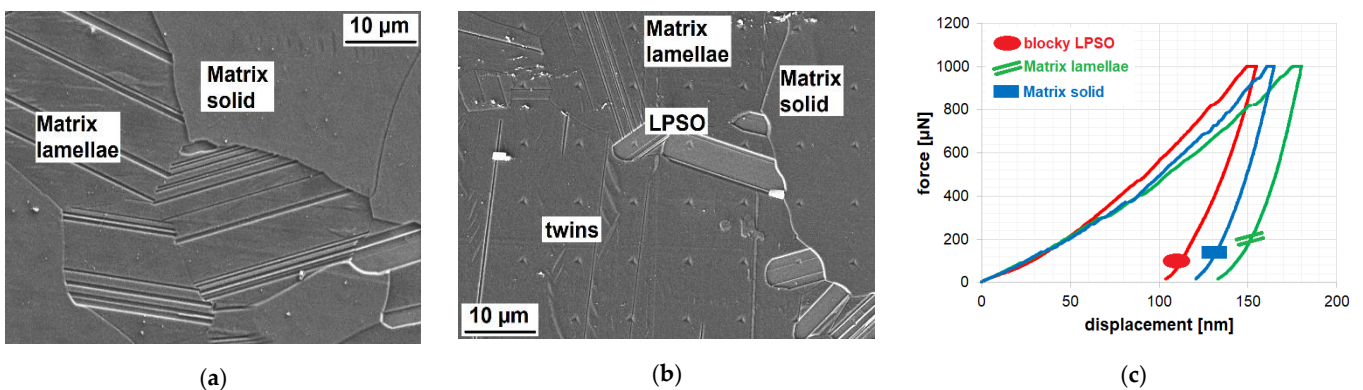


Figure 3. SEM micrographs of Mg-Dy-Nd-Zn-Zr alloy after heat treatment at 500 °C for (a) 120 h and (b) 96 h—magnified section of Figure 2a—and followed by quenching in 55 °C warm water. (c) Force–displacement curve of blocky LPSO and Mg matrix grains with LPSO lamellae and without obvious LPSO lamellae (solid), taken from indents shown in Figure 3b.

The bar charts in Figure 4 show the dependence of the grain size on the heat treatment duration compared to the extruded state. The grain size increases during solution heat treatment up to $43.8 \pm 27.7 \mu\text{m}$ at 72 h and then decreases towards longer heat treatment

durations, see Figure 4a. The overall nanohardness (average of all hardness values) also shows a peak value, and at 24 h a value of 1.74 ± 0.19 GPa is reached, as seen in Figure 4b. Figure 4c shows that the area fraction of Mg matrix grains with LPSO lamellae becomes higher with increasing solution heat treatment duration: solution heat treating for 0.5 h results in 45% of grains showing LPSO lamellae; this value increases to 73% for 120 h, which is higher than that for the as-extruded state (68%). The bar chart in Figure 4d shows the nanohardness values separated in Mg matrix grains with and without LPSO lamellae (mostly measured in the Mg matrix in between the LPSO lamellae), where the grain without LPSO lamellae shows higher values. However, an indent directly at an LPSO lamellae shows high hardness values, whereas nearby or at the edge there is a lower hardness value.

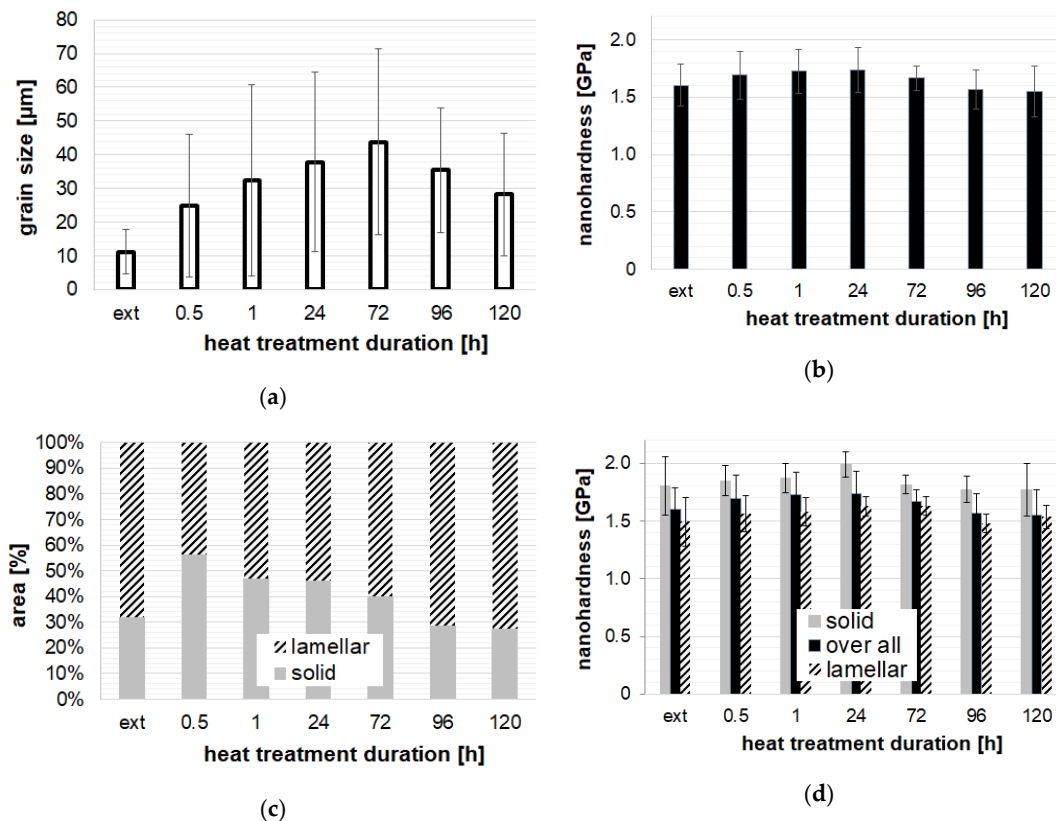


Figure 4. Microstructure depending on (a) grain size, (b) overall nanohardness, (c) area fraction of Mg matrix grains without LPSO lamellae (solid) and with LPSO lamellae, and (d) nanohardness of individual grains compared to overall hardness: Mg matrix grains with LPSO lamellae and without obvious LPSO lamellae (solid)-solution heat treatment and quenched in 55 °C water (numbers stand for heat treatment duration).

The graphs in Figure 5a–d show clustered nanohardness values of indents in blocky LPSO phases, presented in red and classified first; shown are Mg matrix grains including indents direct at LPSO lamellae (separated provided and shown by an example in Figure 3b: bottom row, second indent from the left), presented in green; also shown are Mg matrix grains without obvious LPSO lamellae, presented in blue (“Matrix solid”). Each cluster belongs to one grain. The blocky LPSO show the highest hardness values for all solution heat treatment durations (24 h, 72 h, 96 h and 120 h), and the Mg matrix grains without obvious LPSO phases (Matrix solid) show higher hardness values than the LPSO lamellae-containing grains. However, the difference reduces towards longer heat treatment durations, as does the number of indents in grains free of LPSO lamellae (see area fraction in Figure 4c).

Even though the nanohardness of the blocky LPSO phases after solution heat treatment of 72 h was found to be 2.41 ± 0.30 GPa, and after 96 h was read at 1.84 ± 0.48 GPa, the

nanohardness of the blocky LPSO phases decrease in an overall trend with increasing heat treatment duration. The nanohardness of the blocky LPSO phases in the as-extruded state was found to be 2.43 ± 0.21 GPa, and after solution heat treatment of 120 h a nanohardness of 2.21 ± 0.37 GPa was established.

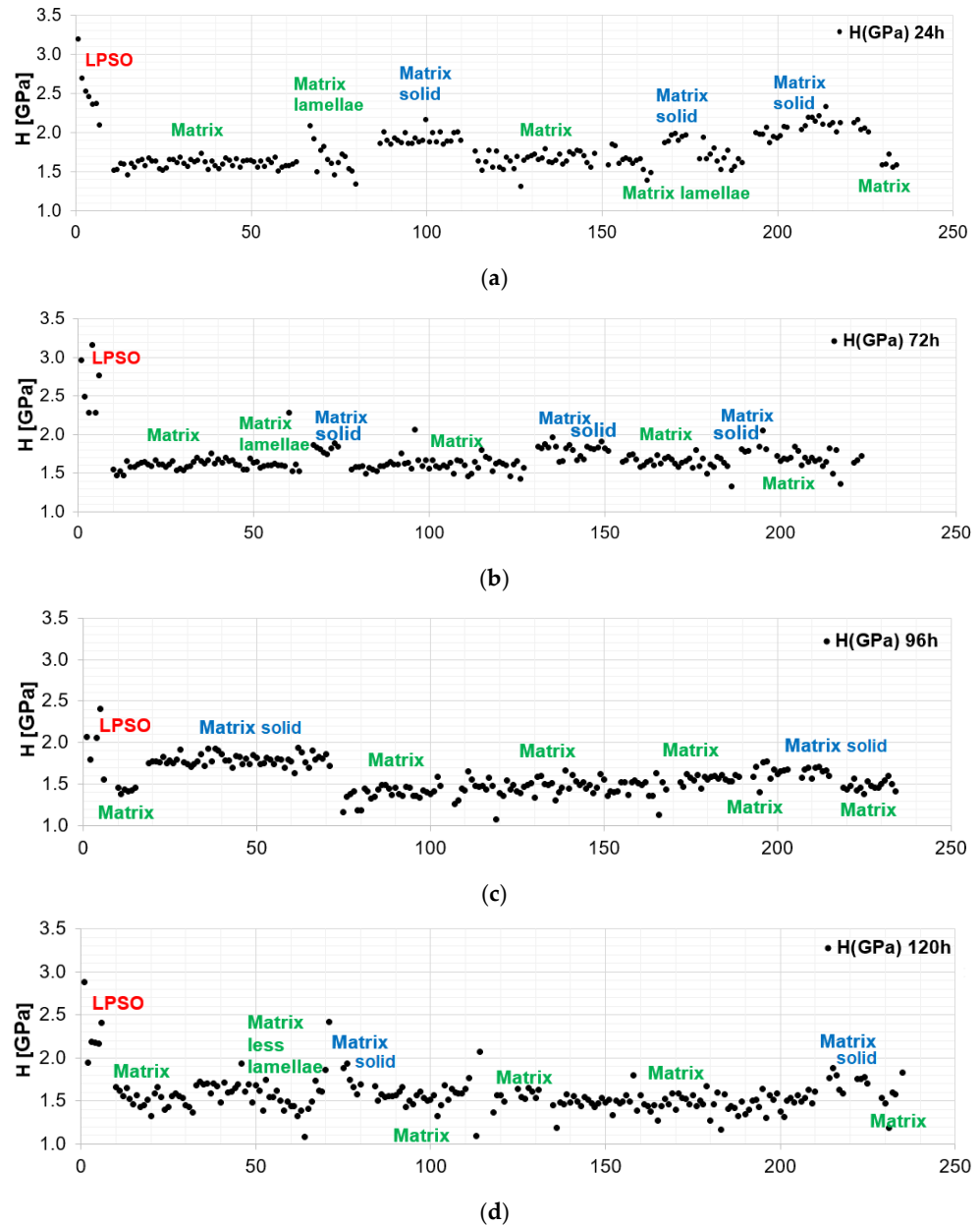


Figure 5. Nanohardness of individual indents organized according to the grains and locations they belong to. The first classified group comprises indents (<10) within the blocky LPSO phases, followed by Mg grains without LPSO lamellae (Matrix solid) and Mg matrix with LPSO lamellae, at different heat treatment durations: (a) 24 h, (b) 72 h, (c) 96 h and (d) 120 h.

To investigate the influence of the cooling rate, the samples heat-treated for 0.5 h and 1 h were, beside quenching in 55 °C warm water, also cooled in air. Figure 6a,b show the microstructure, observed by light microscopy, and Figures 7a–c and 8 present the grain size, number of LPSO phases and grains with and without LPSO lamellae as well as nanohardness compared to the data for quenching in 55 °C warm water. According to Figure 7a, the grain size increases towards the solution heat treatment duration and in water quenching conditions, whereas the number of blocky phases reduces (Figure 7b).

Figure 7b shows that the number of grains per area of Mg matrix grains with LPSO lamellae is slightly higher in water quenching conditions and at 1 h heat-treating.

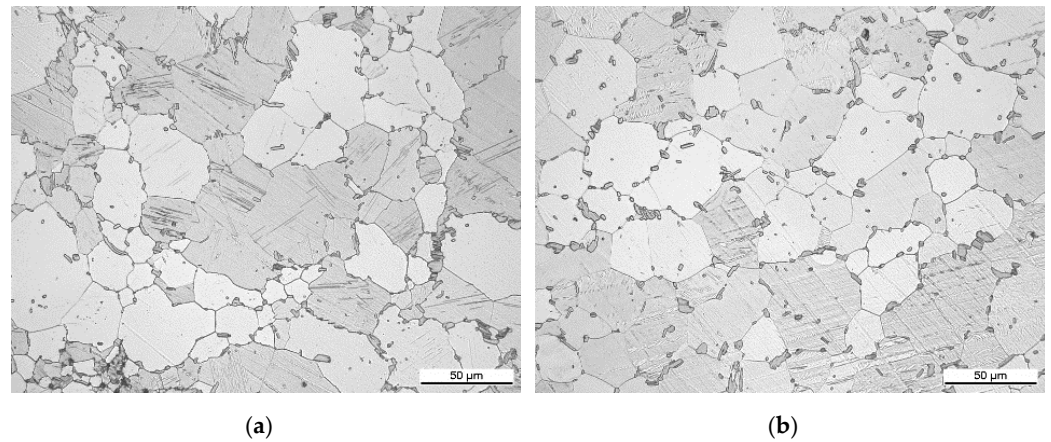


Figure 6. Micrographs of Mg-Dy-Nd-Zn-Zr alloy after heat treatment at 500 °C for (a) 0.5 h and (b) 1 h followed by cooling in air, showing LPSO lamellae within Mg matrix grains and blocky LPSO within the grain and at grain boundaries in different quantities.

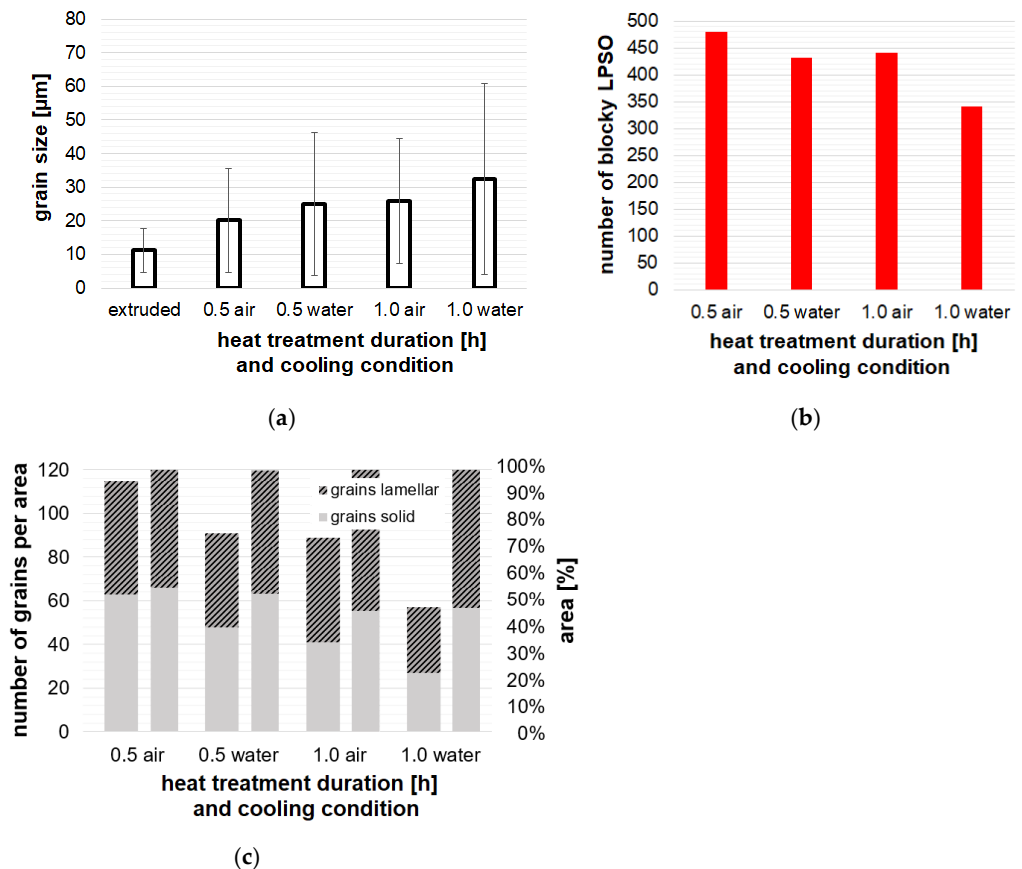


Figure 7. Microstructure depending on (a) grain size, (b) number of blocky LPSO and (c) number of grains per area of Mg matrix grains without LPSO lamellae (solid) and with LPSO lamellae—given solution heat treatment and cooled in air.

The nanohardness of the microstructure after solution heat treatment and cooling in air for grains classified into Mg matrix grains, both with LPSO lamellae and without obvious LPSO lamellae (solid), is shown in Figure 8 (note that the x axis starts at 1.1 GPa) and compared to overall hardness, as well as to the nanohardness of the as-extruded state.

Taking the error bars into account, the difference is very small—however, there is a slight increase in nanohardness for “solid” grains in the water quenched microstructure compared to cooling in air and compared with the average/overall value (black bars).

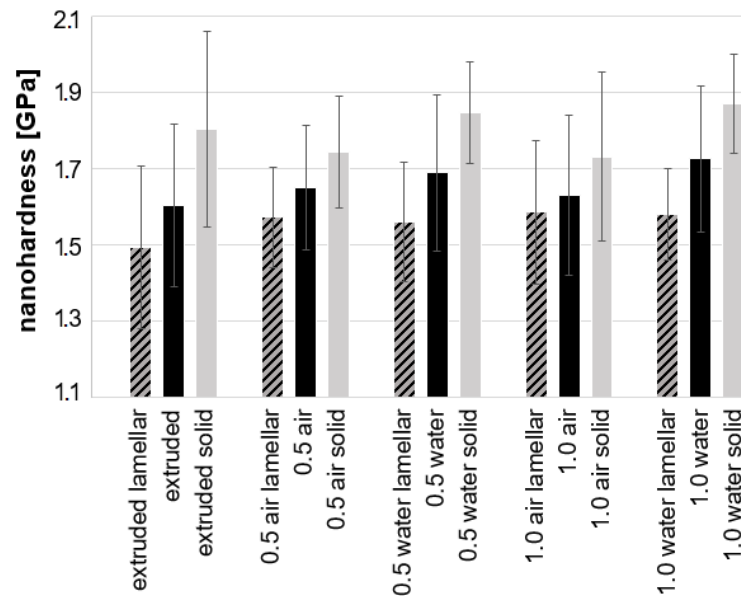


Figure 8. Nanohardness of individual grains clustered to Mg matrix grains with LPSO lamellae and without obvious LPSO lamellae (solid) compared to overall hardness—given solution heat treatment and cooled in air and water quenched (numbers stand for heat treatment duration).

4. Discussion

Similar to reports of others [4,11,20] the as-extruded microstructure of the Mg-Dy-Nd-Zn-Zr alloy used in this study consists of Mg grains with LPSO lamellae in a parallel arrangement throughout the single grains (either seen by the lamellae itself or by the grey, darker appearance of the Mg grains), blocky LPSO phases within the Mg grains, mostly at the grain boundaries and Mg grains free of LPSO lamellae (which appear very bright). As described in the literature [19], all alloying elements in these “brighter” grains are expected to be in solid solution. According to Figure 1a, the area fraction of the grains free of LPSO lamellae is estimated to be less than 20%. Solution heat treatment shows grain growth already after 0.5 h, with an increase up to a duration of 72 h. This goes along with a reduction of blocky LPSO phases [see also 43] and growing amount of LPSO lamellae within the Mg grains. This shows that solid solution heat treatment causes a dissolution of the blocky LPSO phases and a precipitation of LPSO lamellae, as has also been reported by [2,10,12,25]. The blocky phases reduce slightly in nanohardness during dissolution. An increasing amount of LPSO lamellae seem to trigger the formation of new grains: at 96 h and 120 h, a decreasing grain size has been found. This is usually only found after deformation and recrystallization. Zhang et al. [4] and Liu et al. [45] found that LPSO phases (fragmented LPSO lamellae) trigger the particle-stimulated nucleation mechanism and that the newly formed grains are free of LPSO lamellae. This may be the reason why the ratio of the Mg grains with and without LPSO lamellae hardly changes towards 120 h (~30%/~70%)—the new grains forming are rather free of LPSO lamellae, while the existing grains are assumed to contain increasing amounts of LPSO phase.

Our results make clear that the blocky LPSO phases have the highest hardness and that the grains without obvious LPSO lamellae are harder than the grains with LPSO lamellae. Additionally, according to [43], the Mg matrix in between LPSO lamellae shows the smallest hardness value. That means that even with the LPSO lamellae within the grains, which can be when closely indented be much harder than the “in between Mg matrix”, these grains do not reach the hardness value of the solid solution state. Towards the heat treatment duration of 24 h the overall nanohardness reaches a peak value of 1.74 ± 0.19 GPa. Interestingly, this

peak value is nearly reached already after 1 h (1.73 ± 0.19 GPa). With further increasing heat treatment duration, the overall hardness decreases. Due to the lower area fraction of the harder Mg grains in a solid solution state, they provide a smaller contribution to the overall value, and they even decrease in area fraction and hardness with increasing heat treatment duration up to 96 h. Agreeing to the similar results for 96 h and 120 h according to the area fraction, the hardness values also do not change much. It seems that the microstructure has reached a homogenization stage: the overall hardness comes the closest to the hardness values of the Mg matrix grains with LPSO lamellae. It should be pointed out that the hardness values are sensitive to the (sub)surface condition. Even dislocations in the sub-surface range can generate a variance.

It can be concluded that the microstructure does not cause significant pop-ins, the force-displacement curves show small pop-in, but not in an amount and degree known from Mg-alloys, when twinning under nanoindentation or consisting of inhomogeneously distributed particles [46–48]. The twins seen in the microstructure are not from nanoindentation itself, but rather they have been in the microstructure from either extrusion or preparation. The results reveal no apparent discontinuities within the microstructure (the influence of the Mg hydrides are excluded from this discussion and they rather cause sliding along the surface than pop-in, also resulting in wrong hardness values). The small amount of strain-bursts, caused by accumulation of dislocation [49], are in a similar amount in grains with or without LPSO lamellae or even in blocky LPSO phases.

When paying attention to different cooling conditions, we expected different results, in accordance with the results in [42]: a higher amount of precipitated LPSO lamellae for slow cooling. However, first we need to clarify that quenching in 55 °C warm water left the sample longer at a “higher” temperature (a few minutes) than cooling in air: here, room temperature was reached within seconds, due to the small size of the samples. So, cooling in air has the faster cooling rate or, in other words, the shorter exposure to a “higher” temperature. This short variation in temperature exposure did not make a difference to the ratio of the Mg grains with and without LPSO lamellae (for 0.5 h: 55%/45%), but slightly on the average grain size and number of blocky LPSO phases. Both increasing grain size and reduction in numbers of blocky LPSO phases agree with the trend seen up to 72 h. The microstructure consisting of Mg grains with and without LPSO lamellae changes also slightly from 0.5 h to 1 h heat-treating: the number of grains with LPSO lamellae increases. So, in agreement to the as-cast state in [42] the grains become larger with increasing heat treatment duration and slow cooling, leading to additional grain growth. What we learnt is that none of the two cooling conditions lead to a microstructure, whereas all the grains consist of LPSO lamellae. This constitutes a clear difference between initially starting with as-cast and as-extruded states, like also seen in [10]. The nanohardness does not differ much due to either heat treating for 0.5 h or 1.0 h or cooling in air or water, but some small changes are found and the slightly higher nanohardness values of the Mg grains free of LPSO lamellae in the water quenched microstructure will be some result of ongoing solid solution strengthening. Since at this low heat treatment duration the area fraction of Mg grains free of LPSO phases is still near 50%, their nanohardness values play a bigger role on the overall nanohardness than seen after long heat treatment durations with ~30% area fraction. The determination of hardness by nanoindentation has proven to be a good method to make small local hardness changes determinable and to nanomechanically accompany the transformation of LPSO phases by solid solution heat treatment.

5. Conclusions

The study of nanomechanical analysis of an extruded and heat-treated Mg-Dy-Nd-Zn-Zr alloy in correlation with microstructural changes during solution annealing allows the following conclusions: (1) the initially fine-grained microstructure with blocky and lamellar LPSO structures within the Mg matrix and blocky LPSO phases at the grain boundaries first transformed into coarser grains with fewer LPSO lamellae, whose amount then increased again at higher annealing durations, accompanied by decreasing grain

size. (2) The blocky LPSO phases, which have the highest hardness compared to the matrix grains, steadily decrease in quantity, as does the trend of their hardness value. (3) The Mg matrix grains with LPSO lamellae show a lower hardness compared to the Mg matrix grains without or with only a few lamellar LPSO phases as with increasing annealing durations the microstructure homogenizes with respect to the nanohardness values. (4) For long heat treatment durations, the overall hardness of the microstructure is essentially determined by the grains containing LPSO lamellae, since their area fraction is 70%; for short heat treatment durations, the hardness value is influenced proportionally. (5) The overall nanohardness reaches the highest value at 24 h and the grain size does so slightly later at 72 h, as decreasing nanohardness after reaching the peak value goes along with an increasing amount of LPSO lamellae. (6) Cooling in air and quenching in 55 °C for 0.5 h and 1.0 h water influences the microstructure and nanohardness—showing that nanoindentation offers the possibility to determine small changes in solid solution strengthening. (7) The extruded Mg-Dy-Nd-Zn-Zr alloy first undergoes a dissolution of LPSO lamellae, followed by re-precipitation. Finally (8), the LPSO lamellae-containing microstructure does not lead to remarkable pop-in effects.

Author Contributions: Conceptualization, P.M.; methodology, M.S. and P.M.; validation, P.M.; formal analysis, P.M.; investigation, M.S., C.J. and B.C.; data curation, M.S. and P.M.; writing—original draft preparation, P.M.; writing—review and editing, P.M. and C.F.; visualization, P.M.; supervision, C.F. All authors have read and agreed to the published version of the manuscript.

Funding: This research received no external funding.

Data Availability Statement: Not applicable.

Acknowledgments: The authors kindly acknowledge the support given MeKo Manufacturing e.K., Germany and Helmholtz-Center Hereon, Germany, by providing the material.

Conflicts of Interest: The authors declare no conflict of interest.

References

1. Kawamura, Y.; Yamasaki, M. Formation and Mechanical Properties of Mg₉₇Zn₁RE₂ Alloys with Long-Period Stacking Ordered Structure. *Mater. Trans.* **2017**, *48*, 2986–2992. [[CrossRef](#)]
2. Bi, G.; Han, Y.; Jiang, J.; Li, Y.; Zhang, D.; Qiu, D.; Easton, M. Microstructure and mechanical properties of an extruded Mg-Dy-Ni alloy. *Mater. Sci. Eng. A* **2019**, *760*, 246–257. [[CrossRef](#)]
3. Wang, K.; Dou, X.; Wang, J.; Huang, Y.; Gavras, S.; Hort, N.; Liu, S.; Hu, H.; Wang, J.; Pan, F. Achieving enhanced mechanical properties in Mg-Gd-Y-Zn-Mn alloy by altering dynamic recrystallization behavior via pre-ageing treatment. *Mater. Sci. Eng. A* **2020**, *790*, 139635. [[CrossRef](#)]
4. Zhang, Z.; Du, Y.; Zhang, G.; Yan, Z.; Yu, J.; Meng, M. Microstructure and Mechanical Properties of MgGdYZnZr Alloy Prepared by Repetitive Upsetting and Extrusion. *Mater. Trans.* **2018**, *59*, 669–673. [[CrossRef](#)]
5. Ramezani, S.M.; Zarei-Hanzaki, A.; Abedi, H.R.; Salandari-Rabori, A.; Minarik, P. Achievement of fine-grained bimodal microstructures and superior mechanical properties in a multi-axially forged GWZ magnesium alloy containing LPSO structures. *J. Alloys Compd.* **2019**, *793*, 134–145. [[CrossRef](#)]
6. Xu, D.; Han, E.; Xu, Y. Effect of long-period stacking ordered phase on microstructure, mechanical property and corrosion resistance of Mg alloys: A review. *Prog. Nat. Sci. Mater. Int.* **2016**, *26*, 117–128. [[CrossRef](#)]
7. Sun, C.; Liu, H.; Wang, C.; Ju, J.; Bai, J.; Xue, F.; Ma, A.; Jiang, J.; Chen, X.B. Fragmentation of 18R LPSO phases through multi-pass equal channel angular pressing and its impact on rollability of Mg₉₇Y₂Zn₁ (at%) alloy. *J. Mater. Res. Technol.* **2020**, *9*, 14865–14877. [[CrossRef](#)]
8. Zheng, L.; Zhang, X.; Wang, H.; Wang, L.; Hou, H.; Li, H.; Kwang, S. Synergistic effect of LPSO and eutectic phase on mechanical properties of Mg-Gd-Nd-Zn-Zr alloy during equal channel angular pressing. *J. Mater. Res. Technol.* **2021**, *15*, 2459–2470. [[CrossRef](#)]
9. Li, Y.X.; Qiu, D.; Rong, Y.H.; Zhang, M.X. Effect of long-period stacking ordered phase on thermal stability of refined grains in Mg-RE-based alloys. *Philos. Mag.* **2014**, *94*, 1311–1326. [[CrossRef](#)]
10. Liu, H.; Bai, J.; Yan, K.; Yan, J.; Ma, A.; Jiang, J. Comparative studies on evolution behaviors of 14H LPSO precipitates in as-cast and as-extruded Mg-Y-Zn alloys during annealing at 773K. *Mater. Des.* **2016**, *93*, 9–18. [[CrossRef](#)]
11. Xu, P.; Yu, J.; Zhang, Z. Microstructure and Texture Evolution of Mg-Gd-Y-Zn-Zr Alloy by Compression-Torsion Deformation. *Materials* **2019**, *12*, 2773. [[CrossRef](#)]
12. Kittner, K.; Ullmann, M.; Arndt, F.; Kawalla, R.; Prahl, U. Microstructure and Texture Evolution during Twin-Roll Casting and Annealing of a Mg-6.8Y-2.5Zn-0.4Zr Alloy (WZ73). *Crystals* **2020**, *10*, 513. [[CrossRef](#)]

13. Liao, H.; Kim, J.; Lee, T.; Song, J.; Peng, J.; Jiang, B.; Pan, F. Effect of heat treatment on LPSO morphology and mechanical properties of Mg–Zn–Y–Gd alloys. *J. Magnes. Alloys* **2020**, *8*, 1120–1127. [[CrossRef](#)]
14. Wang, D.; Wu, H.; Wu, R.; Wang, Y.; Zhang, J.; Betsofen, S.; Krit, B.; Hou, L.; Nodir, T. The transformation of LPSO type in Mg-4Y-2Er-2Zn-0.6Zr and its response to the mechanical properties and damping capacities. *J. Magnes. Alloys* **2020**, *8*, 793–798. [[CrossRef](#)]
15. Lu, R.; Jiao, K.; Zhao, Y.; Li, K.; Yao, K.; Hou, H. A Study on the Damping Capacities of Mg–Zn–Y-Based Alloys with Lamellar Long Period Stacking Ordered Phases by Preparation Process. *Metals* **2021**, *11*, 79. [[CrossRef](#)]
16. Wu, Y.J.; Zeng, X.Q.; Lin, D.L.; Peng, L.M.; Ding, W.J. The microstructure evolution with lamellar 14H-type LPSO structure in an Mg_{96.5}Gd_{2.5}Zn₁ alloy during solid solution heat treatment at 773K. *J. Alloys Compd.* **2009**, *477*, 193–197. [[CrossRef](#)]
17. Ding, W.J.; Wu, Y.J.; Peng, L.M.; Zeng, X.Q.; Yuan, G.Y.; Lin, D.L. Formation of 14H-type long period stacking ordered structure in the as-cast and solid solution treated Mg–Gd–Zn–Zr alloys. *J. Mater. Res.* **2009**, *24*, 1842–1854. [[CrossRef](#)]
18. Xu, C.; Nakata, T.; Qiao, X.; Zheng, M.; Wu, K.; Kamado, S. Effect of LPSO and SFs on microstructure evolution and mechanical properties of Mg–Gd–Y–Zn–Zr alloy. *Sci. Rep.* **2017**, *7*, 40846. [[CrossRef](#)]
19. Liu, H.; Ju, J.; Bai, J.; Sun, J.; Song, D.; Yan, J.; Jiang, J.; Ma, A. Preparation, Microstructure Evolutions, and Mechanical Property of an Ultra-Fine Grained Mg-10Gd-4Y-1.5Zn-0.5Zr Alloy. *Metals* **2017**, *7*, 398. [[CrossRef](#)]
20. Liu, W.; Zhang, J.; Xu, C.; Zong, X.; Zhush, W.; Ma, Q. Precipitation behaviors of 14H LPSO lamellae in Mg₉₆Gd₃Zn_{0.5}Ni_{0.5} alloys during severe plastic deformation. *J. Mater. Sci.* **2017**, *52*, 13271–13283. [[CrossRef](#)]
21. Dong, B.; Zhang, Z.; Che, X.; Yu, J.; Meng, M.; Zhang, J. Microstructure, Texture Evolution, and Mechanical Properties of MDFed GWZ Alloy Containing LPSO Phases on the Condition of High and Low Temperature Cycle Deformation. *Metals* **2020**, *10*, 136. [[CrossRef](#)]
22. Yuan, J.; Li, T.; Zhang, K.; Li, X.; Li, Y.; Ma, M.; Shi, G.; Du, Z.; Liu, W.; Peng, Y. Precipitation Behavior of Mg-7Gd-3Y-2Zn-0.5Zr Alloy during Isothermal Aging. *Materials* **2021**, *14*, 1737. [[CrossRef](#)] [[PubMed](#)]
23. Wang, G.; Xiao, Z.; Yang, Z.; Liu, P. The evolution of LPSO phase and its influence on grain size during cooling free forging. *Mater. Res. Express* **2021**, *8*, 76508. [[CrossRef](#)]
24. CAI, X.; Fu, H.; Guo, J.; Peng, Q. Negative Strain-Rate Sensitivity of Mg Alloys Containing 18R and 14H Long-Period Stacking-Ordered Phases at Intermediate Temperatures. *Metall. Mater. Trans. A* **2014**, *45*, 3703–3707. [[CrossRef](#)]
25. Yuan, L.; Bi, G.; Li, Y.; Jiang, J.; Han, Y.; Fang, D.; Ma, Y. Effects of solid solution treatment and cooling on morphology of LPSO phase and precipitation hardening behavior of Mg–Dy–Ni alloy. *Trans. Nonferrous Met. Soc. China* **2017**, *27*, 2381–2389. [[CrossRef](#)]
26. Egusa, D.; Abe, E. The structure of long period stacking/order Mg–Zn–RE phases with extended non-stoichiometry ranges. *Acta Mater.* **2012**, *60*, 166–178. [[CrossRef](#)]
27. Zhang, J.; Liu, S.; Wu, R.; Hou, L.; Zhang, M. Recent developments in high-strength Mg-RE-based alloys: Focusing on Mg-Gd and Mg-Y systems. *J. Magnes. Alloys* **2018**, *6*, 277–291. [[CrossRef](#)]
28. Sun, W.T.; Qiao, X.G.; Zheng, M.Y.; Hu, N.; Gao, N.; Starink, M.J. Evolution of long-period stacking ordered structure and hardness of Mg-8.2Gd-3.8Y-1.0Zn-0.4Zr alloy during processing by high pressure torsion. *Mater. Sci. Eng. A* **2018**, *738*, 238–252. [[CrossRef](#)]
29. Schuh, C.A. Nanoindentation studies of materials. *Mater. Today* **2006**, *9*, 32–40. [[CrossRef](#)]
30. Bočan, J.; Maňák, J.; Jäger, A. Nanomechanical analysis of AZ31 magnesium alloy and pure magnesium correlated with crystallographic orientation. *Mater. Sci. Eng. A* **2015**, *644*, 121–128. [[CrossRef](#)]
31. Lu, Y.; Ding, R.G.; Chiu, Y.L.; Jones, I.P. Tomographic investigation of the effects of second phases on the biodegradation and nano-mechanical performance of a Mg–Zn–Ca alloy. *Materialia* **2018**, *4*, 1–9. [[CrossRef](#)]
32. Ghasemi, A.; Penther, D.; Kamrani, S. Microstructure and nanoindentation analysis of Mg-SiC nanocomposite powders synthesized by mechanical milling. *Mater. Charact.* **2018**, *142*, 137–143. [[CrossRef](#)]
33. Li, D.; Zhang, J.; Que, Z.; Xu, C.; Niu, X. Effects of Mn on the microstructure and mechanical properties of long period stacking ordered Mg₉₅Zn_{2.5}Y_{2.5} alloy. *Mater. Lett.* **2013**, *109*, 46–50. [[CrossRef](#)]
34. Zhang, Z.; Zhang, Y.; Zhang, J.; Li, Y.; Ma, Y.; Xu, C. Effect of ZRB2-modified on microstructure and mechanical properties of Mg-Zn-Y-Mn alloy. *J. Magnes. Alloys* **2018**, *6*, 255–262. [[CrossRef](#)]
35. Zhang, H.X.; Chen, S.F.; Cheng, M.; Zheng, C.; Zhang, S.H. Modeling the Dynamic Recrystallization of Mg–11Gd–4Y–2Zn–0.4Zr Alloy Considering Non-uniform Deformation and LPSO Kinking During Hot Compression. *Acta Metall. Sin. Engl. Lett.* **2019**, *32*, 1122–1134. [[CrossRef](#)]
36. Zhang, X.; Sun, G.; Liu, J.; Che, C.; Yang, M.; Han, S.; Fang, D.; Jiang, Z.; Lian, J. Effect of Zn addition on the microstructures and mechanical behaviors of As-cast Mg-2.5Y-1Ce-0.5Mn alloy. *Mater. Res. Express* **2020**, *1*, 7. [[CrossRef](#)]
37. MeKo Manufacturing, e.K. Available online: www.meko.de/RESOLOY (accessed on 12 October 2022).
38. Fort Wayne Metals. Available online: www.fwmetals.com/RESOLOY-a-magnesium-alloy-for-absorbable-devices (accessed on 12 October 2022).
39. Maier, P.; Griebel, A.; Jahn, M.; Bechly, M.; Menze, R.; Bittner, B.; Schaffer, J. Corrosion Bending Fatigue of RESOLOY[®] and WE43 Magnesium Alloy Wires. In *Magnesium Technology 2019; The Minerals Metals & Materials Series*; Joshi, V., Jordon, J., Orlov, D., Neelameggham, N.R., Eds.; Springer: Cham, Switzerland, 2019; pp. 175–181. [[CrossRef](#)]

40. Yang, L.; Huang, Y.; Feyerabend, F.; Willumeit, R.; Mendis, C.; Kainer, K.U.; Hort, N. Microstructure, mechanical and corrosion properties of Mg–Dy–Gd–Zr alloys for medical applications. *Acta Biomater.* **2013**, *9*, 8499–8508. [[CrossRef](#)]
41. Feyerabend, F.; Fischer, J.; Holtz, J.; Witte, F.; Willumeit, R.; Drücker, H.; Vogt, C.; Hort, N. Evaluation of short-term effects of rare earth and other elements used in magnesium alloys on primary cells and cell lines. *Acta Biomater.* **2010**, *6*, 1834–1842. [[CrossRef](#)]
42. Ahlers, S.; Bittner, B.; Maier, P. Influence of Cooling Conditions on Long-Period Stacking-Ordered Phase Evolution and Corrosion Behavior of As-Cast Resoloy[®]. *Metals* **2021**, *11*, 1372. [[CrossRef](#)]
43. Maier, P.; Clausius, B.; Richter, A.; Bittner, B.; Hort, N.; Menze, R. Crack Propagation in As-Extruded and Heat-Treated Mg–Dy–Nd–Zn–Zr Alloy Explained by the Effect of LPSO Structures and Their Micro- and Nanohardness. *Materials* **2021**, *14*, 3686. [[CrossRef](#)]
44. Huang, Y.; Yang, L.; You, S.; Gan, W.; Kainer, K.U.; Hort, N. Unexpected formation of hydrides in heavy rare earth containing magnesium alloys. *J. Magnes. Alloys* **2016**, *4*, 173–180. [[CrossRef](#)]
45. Liu, H.; Meng, Y.; Yu, H.; Xu, W.; Zhang, S.; Jia, L.; Wu, G. The Role of Long Period Stacking Ordered Phase in Dynamic Recrystallization of a Mg–Gd–Y–Zn–Zr Alloy during Multi-Directional Forging Process. *Materials* **2020**, *13*, 3290. [[CrossRef](#)] [[PubMed](#)]
46. Cheng, J.; Guo, T.; Barnett, M.R. Influence of temperature on twinning dominated pop-ins during nanoindentation of a magnesium single crystal. *J. Magnes. Alloys* **2022**, *10*, 169–179. [[CrossRef](#)]
47. Hu, J.; Zhang, W.; Peng, G.; Zhang, T.; Zhang, Y. Nanoindentation deformation of refine-grained AZ31 magnesium alloy: Indentation size effect, pop-in effect and creep behavior. *Mater. Sci. Eng. A* **2018**, *725*, 522–529. [[CrossRef](#)]
48. Huang, C.-Y.; Hsieh, P.-J.; Chen, I.-C.; Ke, W.-C.; Yang, P.-F.; Jian, S.-R. Nanoindentation of Mg-doped AlGaIn thin films. *J. Alloys Compd.* **2014**, *593*, 220–223. [[CrossRef](#)]
49. Sato, Y.; Shinzato, S.; Ohmura, T.; Hatano, T.; Ogata, S. Unique universal scaling in nanoindentation pop-ins. *Nat. Commun.* **2020**, *11*, 4177. [[CrossRef](#)]